Biochimica et Biophysica Acta 1828 (2013) 2628–2636

Contents lists available at ScienceDirect

Biochimica et Biophysica Acta

journal homepage: www.elsevier.com/locate/bbamem

Aggregates of nisin with various bactoprenol-containing cell wall precursors differ in size and membrane permeation capacity

Katharina Scherer [a,*], Imke Wiedemann [b,1], Corina Ciobanasu [a], Hans-Georg Sahl [b], Ulrich Kubitscheck [a]

[a] Institute for Physical and Theoretical Chemistry, Wegeler Str. 12, Rheinische Friedrich-Wilhelms-University Bonn, 53115 Bonn, Germany
[b] Institute for Medical Microbiology, Immunology and Parasitology, Pharmaceutical Microbiology Unit, Meckenheimer Allee 168, Rheinische Friedrich-Wilhelms-University Bonn, 53115 Bonn, Germany

ARTICLE INFO

Article history:
Received 15 April 2013
Received in revised form 1 July 2013
Accepted 10 July 2013
Available online 18 July 2013

Keywords:
Nisin
Lipid II
Cell wall precursor
Giant unilamellar vesicles
Confocal microscopy
Membrane pore formation

ABSTRACT

Many lantibiotics use the membrane bound cell wall precursor Lipid II as a specific target for killing Gram-positive bacteria. Binding of Lipid II usually impedes cell wall biosynthesis, however, some elongated lantibiotics such as nisin, use Lipid II also as a docking molecule for pore formation in bacterial membranes. Although the unique nisin pore formation can be analyzed in Lipid II-doped vesicles, mechanistic details remain elusive. We used optical sectioning microscopy to directly visualize the interaction of fluorescently labeled nisin with membranes of giant unilamellar vesicles containing Lipid II and its various bactoprenol precursors. We quantitatively analyzed the binding and permeation capacity of nisin when applied at nanomolar concentrations. Specific interactions with Lipid I, Lipid II and bactoprenol-diphosphate (C_{55}-PP), but not bactoprenol-phosphate (C_{55}-P), resulted in the formation of large molecular aggregates. For Lipid II, we demonstrated the presence of both nisin and Lipid II in these aggregates. Membrane permeation induced by nisin was observed in the presence of Lipid I and Lipid II, but not in the presence of C_{55}-PP. Notably, the size of the C_{55}-PP–nisin aggregates was significantly smaller than that of the aggregates formed with Lipid I and Lipid II. We conclude that the membrane permeation capacity of nisin is determined by the size of the bactoprenol-containing aggregates in the membrane. Notably, transmitted light images indicated that the formation of large aggregates led to a pinch-off of small vesicles, a mechanism, which probably limits the growth of aggregates and induces membrane leakage.

1. Introduction

The antimicrobial peptide nisin is produced by many strains of *Lactococcus lactis* and is active against a broad range of Gram-positive bacteria [1,2]. Nisin belongs to the group of lantibiotics, which are characterized by intramolecular rings formed by the thioether amino acids lanthionine and 3-methyllanthionine [3,4]. The peptide is a member of the subgroup of type-A lantibiotics consisting of elongated, screw-shaped peptides with a positive net charge.

Positively charged, antimicrobial peptides like nisin have the capacity to adopt an amphipathic structure upon interaction with membranes [5], and it has been suggested that nisin kills bacteria by disturbing the integrity of the cell membrane [6]. Thus, it was shown in model membrane studies that nisin destroys the membrane of small unilamellar vesicles (SUVs) at micromolecular concentrations [7]. However, when applied against Gram-positive bacteria, nisin shows minimal inhibitory concentrations (MICs) in the nanomolar range [8]. This observation argues against a simple membrane perforation mechanism as primary biological effect. In further studies the cell wall precursor Lipid II was identified as a docking molecule. Evidence that this interaction is crucial for killing bacteria was provided when it was shown that the specific interaction of nisin and Lipid II leads to pore formation [4]. *In vitro* studies revealed that nanomolar concentrations of nisin were sufficient to cause membrane perforation in Lipid II-doped vesicles [7].

For bacteria, Lipid II is an indispensable constituent of the cell membrane because it delivers the monomeric peptidoglycan units for the cell wall biosynthesis. This makes it a prominent target for a number

Abbreviations: AF647, Alexa Fluor 647 N-hydroxysuccinimide hydrazide; Atto488-NHS, Atto 488 N-hydroxysuccinimide; CF, 5(6)-carboxyfluorescein; CLSM, confocal laser scanning microscopy; C_{55}-PP, undecaprenyl-diphosphate (bactoprenol-diphosphate); C_{55}-P, undecaprenyl-phosphate (bactoprenol-phosphate); DOPC, 1,2-dioleoyl-*sn*-glycero-3-phosphocholine; DOPG, 1,2-dioleoyl-*sn*-glycero-3-phospho-(1′-*rac*-glycerol) (sodium salt); EDC, 1-ethyl-3-(3-dimethylaminopropyl)carbodiimide; GlcNAc, N-acetylglucosamine; GUV, giant unilamellar vesicle; LI, Lipid I; LII, Lipid II; LSM, laser scanning microscope; LUV, large unilamellar vesicle; LY, Lucifer yellow; MES, 2-(N-morpholino)ethanesulfonic acid; MIC, minimal inhibitory concentration; MurNAc, N-acetylmuramic acid; nisin–AF647, nisin coupled to Alexa Fluor 647; SUV, small unilamellar vesicle; TFA, trifluoroacetic acid; UDP, uridine diphosphate

* Corresponding author at: Rheinische Friedrich-Wilhelms-University Bonn, Institute for Physical and Theoretical Chemistry, Wegelerstr. 12, D-53115 Bonn, Germany. Tel.: +49 228 735693; fax: +49 228 739424.
E-mail addresses: kscherer@uni-bonn.de (K. Scherer), iwiedemann@medpharmaservice.de (I. Wiedemann), corinaciobanasu@yahoo.com (C. Ciobanasu), sahl@mibi03.meb.uni-bonn.de (H.-G. Sahl), u.kubitscheck@uni-bonn.de (U. Kubitscheck).
[1] Present address: MedPharmaService GmbH, Neuköllnische Allee 146, 12057 Berlin, Germany.

0005-2736/$ – see front matter © 2013 Elsevier B.V. All rights reserved.
http://dx.doi.org/10.1016/j.bbamem.2013.07.014

of antibiotics [9]. The molecule consists of a membrane-anchoring hydrocarbon chain, undecaprenyl-phosphate (bactoprenol-phosphate), covalently coupled to the monomeric peptidoglycan unit through a pyrophosphate linker. This unit is the basic building block of the cell wall and consists of the two amino sugars N-acetylglucosamine (GlcNAc) and N-acetylmuramic acid (MurNAc), with a pentapeptide bound to the latter. Lipid II is assembled on the cytosolic face of the membrane by successive enzymatic reactions (Fig. 1). The thereby generated intermediate is named Lipid I, which is composed of undecaprenyl-diphosphate covalently bound to MurNAc. Lipid II then translocates from the cytoplasmic to the external side of the membrane. The mechanism of translocation is not fully understood, but it is known that the integral membrane protein FtsW, an essential cell division protein, induces the trans-bilayer movement of Lipid II in model membranes [10]. On the external face of the membrane the insertion of peptidoglycan-units into the cell wall is catalyzed. The remaining lipid anchor carrying the pyrophosphate, C_{55}-PP, is dephosphorylated to the monophosphate, C_{55}-P, and shuttled back to the cytosolic side of the membrane to start a new synthesis cycle.

The incubation of Gram-positive bacteria with nisin induces membrane perforation, which leads to cell lysis [11]. *In vitro* studies showed that stable membrane gaps with inner diameters of 2–2.5 nm can occur [12]. At saturation the ratio of nisin molecules per Lipid II was proposed to be 2:1 [13]. The specific interaction of nisin and Lipid II leads to the inhibition of cell wall biosynthesis as Lipid II is bound by nisin and subsequently removed from the reaction cycle. Remarkably, when the interaction of nisin with the bacterial membrane was directly observed by using fluorescently labeled nisin, the peptides were not homogeneously distributed on the bacterial membrane, but clustered in large aggregates [14]. Clustering was also observed by direct imaging of fluorescent nisin on Lipid II containing giant unilamellar vesicles (GUVs) [14]. The pyrophosphate unit of Lipid II was identified as a possible structural binding motif for nisin, around which two lanthionine rings of the peptide might form a cage structure [15]. Accordingly, binding of nisin to C_{55}-PP was observed, however no nisin-induced membrane permeabilization in C_{55}-PP-doped SUVs did occur [15]. Here, the question remains why the specific binding of nisin to the pyrophosphate does not lead to membrane destabilization.

To gain a deeper insight into the effect of nisin on Lipid II and its bactoprenol precursors we used confocal laser scanning microscopy (CLSM) to directly visualize the interaction of fluorescently labeled nisin with respective GUV membranes. We analyzed quantitatively the binding behavior and permeation capacity of nisin when applied in the MIC range. We discriminated between unspecific and specific interactions, the first driven by electrostatic forces and the latter influenced by the binding sites that were offered to nisin. We found that nisin formed large-scale aggregates when C_{55}-PP, Lipid I or Lipid

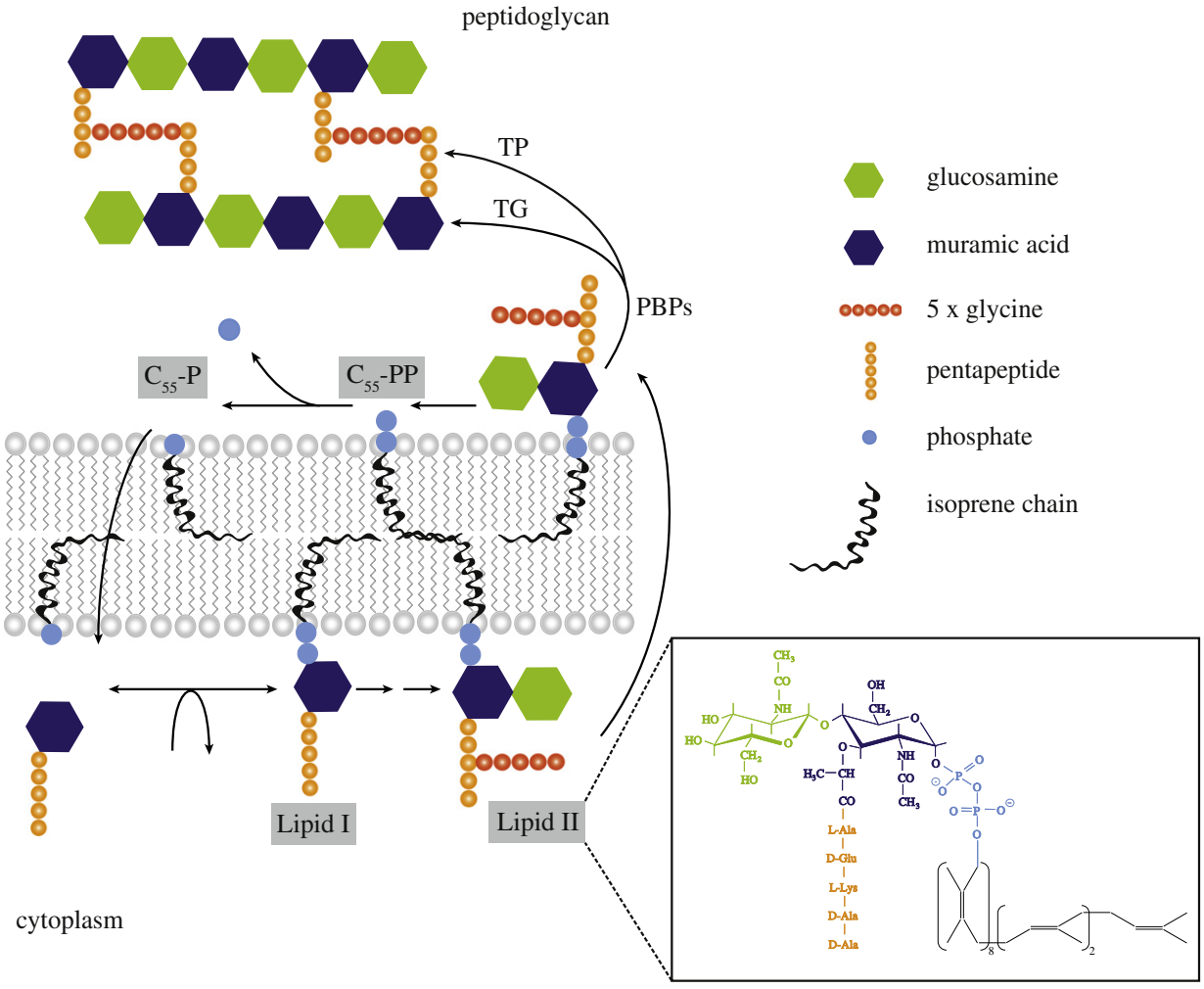

Fig. 1. Cell wall biosynthesis cycle in *S. aureus*. In the first membrane-linked step Lipid I is formed at the inner face of the membrane by coupling the UDP-MurNAc-pentapeptide to the lipid carrier C_{55}-P. Then, through linkage of UDP-GlcNAc to Lipid I, Lipid II is produced. Lipid II translocates across the membrane mediated by the membrane protein FtsW [10]. On the outside, the peptidoglycan unit is incorporated into the peptidoglycan network through the activity of penicillin-binding proteins (PBPs) by transglycosylation (TG) and transpeptidation (TP) reactions. This leaves C_{55}-PP, which is recycled through dephosphorylation, and the retrieved C_{55}-P is available for the next biosynthesis cycle.
Figure modified from [9].

II were present in the membrane. Also, we found that nisin caused membrane permeation when Lipid I or Lipid II were present in the membrane, but not in the presence of C_{55}-PP. Notably, the perforation efficiency correlated with the size of the formed aggregates: Lipid I– and Lipid II–nisin aggregates were comparable in size and about twice as large as C_{55}-PP–nisin aggregates. We concluded that the size of the formed molecular aggregates determined the permeation capacity of nisin. Suspiciously, we observed that at locations of large aggregates in the membrane small vesicles pinched off the GUVs, what might be the physical reason for the membrane permeability in such situations.

2. Material and methods

2.1. Chemicals and materials

All chemicals were of analytical grade or better. The phospholipids 1,2-dioleoyl-*sn*-glycero-3-phosphocholine (DOPC) and 1,2-dioleoyl-*sn*-glycero-3-phospho-(1′-*rac*-glycerol) (sodium salt, DOPG) were purchased from Avanti Polar Lipids (Alabaster, AL, USA) and used without further purification. The lipids were dissolved in chloroform to a final concentration of 1.3 mM. Undecaprenyl-phosphate (C_{55}-P) and undecaprenyl-diphosphate (C_{55}-PP) were purchased from Larodan Fine Chemicals AB (Malmo, Sweden). The hydrophilic dye Lucifer Yellow (LY) was purchased from Invitrogen (Karlsruhe, Germany). Atto488-NHS ester (Sigma Aldrich, Schnelldorf, Germany) and Alexa Fluor 647-hydrazide (Invitrogen, Karlsruhe, Germany) were used for peptide labeling. Nisin Z was purified from culture supernatants of *L. lactis* NIZO22186 [16] by chloroform extraction and HPLC [17]. Nisin Z and nisin A are the two natural mutants of nisin. Nisin Z harbors the amino acid asparagine at position 27 instead of histidine like nisin A. We used nisin Z and simply refer to it as nisin. Purified nisin was lyophilized and stored at −20 °C. Nisin stock solutions were prepared in 0.005% acetic acid at a concentration of 1 mg/ml.

2.2. Synthesis and purification of Lipid I and Lipid II

The lipid-bound cell wall precursor Lipid II was synthesized *in vitro* and purified as described previously [18]. *In vitro* synthesis of Lipid I was achieved by the omission of UDP-GlcNAc from the synthesis assay, and Lipid II-Atto488 by using UDP-MurNAc-pentapeptide-Atto488 instead of the non-labeled substrate. All reaction products were extracted by butanol/6M pyridine acetate pH 4.2 and analyzed by thin layer chromatography.

2.3. Labeling of the UDP-MurNAc-pentapeptide

The fluorescent label was attached to the lysine residue of the pentapeptide side chain in the UDP-MurNAc-pentapeptide, which had been isolated and purified from *Staphylococcus simulans 22* as described [19]. For the labeling reaction UDP-MurNAc-pentapeptide was dissolved in 0.1 M sodium bicarbonate/acetonitrile (1:1, v/v). A solution of Atto488-NHS ester was freshly prepared by the addition of dry DMSO (1 mg/250 μl) and added stepwise to the UDP-MurNAc-pentapeptide solution (molar ratio of UDP-MurNAc-pentapeptide:Atto488-NHS ester of 2:1). The reaction mixture was incubated at room temperature for 60 min and overnight at 4 °C under constant stirring, applied to a C18 HPLC column, and purified using the following gradient: in 10 min from 0% to 20% B; 10 min isocratic at 20% B; in 10 min from 20% to 100% B (buffer A: 50 mM ammonium bicarbonate; buffer B: 100% methanol). UDP-MurNAc-pentapeptide-Atto488 containing fractions were lyophilized and stored at −20 °C.

2.4. Production and purification of fluorescently labeled nisin

The carboxyl group of nisin was coupled to Alexa Fluor 647 (AF647) using Alexa Fluor 647-hydrazide in conjunction with the water-soluble carbodiimide EDC. Nisin (5 mg/ml) was dissolved in 0.1 M MES-buffer, pH 4.7–5.5. AF647-hydrazide was dissolved in dry DMSO (1 mg/60 μl) and added to 0.5 ml nisin solution. Immediately before use, a 500 mM EDC solution in 0.1 M MES-buffer was prepared and 14 μl of the EDC solution was added to the reaction mixture, which was incubated over night at room temperature. Nisin–AF647 was purified on a C18 column using a linear gradient from buffer A (water, 0.1% trifluoroacetic acid, TFA) to 100% buffer B (acetonitrile, 0.1% TFA).

2.5. Efflux experiments

Large unilamellar vesicles (LUVs) for carboxyfluorescein efflux experiments were prepared by the extrusion technique as described previously [7]. 2 μmol DOPC and 0.75 μmol Lipid II (0.05 mol%) were mixed in chloroform and the solvent was removed under a nitrogen stream. The dried lipid film was resuspended in 300 μl of buffer (50 mM MES-sodium hydroxide, 100 mM sodium sulfate, pH 5.5), which contained a self-quenched concentration of carboxyfluorescein (50 mM). Lipids and buffer were swayed in a water bath at 30 °C by hand and then mixed thoroughly on a shaker until no lipid film was recognizable at the bottom of the tube anymore. The resulting suspension of liposomes (multilamellar lipid vesicles) was then quick-frozen in liquid nitrogen and thawed again in a water bath at 30 °C. The freeze–thaw cycle was repeated 8–10 times. The resulting multilamellar vesicles were extruded 21 times through 100 nm polycarbonate membranes (Whatman, Kent, UK) by means of a MiniExtruder (Avanti Polar Lipids, Alabaster, AL, USA). Unencapsulated carboxyfluorescein was then removed by gel filtration (Sephadex G-50, medium, Sigma Aldrich, Schnelldorf, Germany). Fluorescence was measured in a glass cuvette (Hellma Analytics, Müllheim, Germany) using a fluorescence spectrophotometer (LS55, PerkinElmer, Waltham, MA, USA, λ_{ex} = 490 nm; λ_{em} = 525 nm). One hundred per cent carboxyfluorescein leakage was determined by adding triton-X100, 1% (v/v).

2.6. GUV preparation

GUVs were created by electro-formation [20,21]. Vesicles containing only phospholipids were formed from pure DOPC or from an 80/20 mixture of DOPC and DOPG. For permeation and binding assays the same mixtures each supplemented with 0.2 mol% C_{55}P, C_{55}PP, Lipid I or Lipid II, respectively, were used. Twenty microliters of the respective lipid mixture in chloroform were deposited on an indium tin oxide coated coverslip (SPI Supplies, West Chester, PA, USA), and then dried in a desiccator under vacuum. The dried lipid film was hydrated with 250 mM sucrose in bi-distilled water as described in [22].

2.7. Sample preparation for confocal microscopy

For measurements, 250 mM glucose in deionized water or buffer (125 mM glucose, 30 mM MES, 35 mM sodium sulfate, pH = 5.8) were mixed with nisin–AF647 and LY before GUV addition. Nisin–AF647 was diluted to a final concentration of 1.5 μM for the observation of non-specific and specific binding. For translocation analysis nisin–AF647 was diluted to 0.2 μM and LY to a concentration of 20 μM. For binding analysis the same nisin–AF647 concentration was used. 50 μl of vesicle bulk solution were transferred into a microscope sample chamber (MatTek, Ashland, MA, USA) containing 200 μl of the respective glucose or buffer solution. The density difference caused GUV sedimentation, so that the liposomes could be examined by CLSM. Data acquisition was started after 3 min incubation time, when the vesicles resided in a stable position at the chamber bottom.

2.8. Confocal laser scanning microscopy (CLSM)

GUV formation, incorporation of Lipid II-Atto488 into GUVs and interactions between GUVs and nisin–AF647 were examined by CLSM

using an LSM 510 Meta (Carl Zeiss MicroImaging GmbH, Jena, Germany) equipped with a water immersion C-Apochromat 40× objective lens (NA 1.2, Corr) and a Plan-Neofluar 20× air objective lens (NA 0.5) at room temperature. LY and Lipid II-Atto488 were excited with the light of an argon ion laser at 488 nm, and nisin–AF647 was excited using a He–Ne laser at 633 nm. Laser beams were directed to the sample by means of a UV/488/543/633 dichroic beam splitter. For fluorescence detection a secondary 545 dichroic beam splitter supplemented with a BP505-550 filter and a LP650 filter were used. For comparative measurements the same settings for illumination intensity and detector gain were applied.

2.9. Image colocalization analysis

Analysis of the two-color images was done using ImageJ [23] with the colocalization highlighter plugin (authored by Christophe Laummonerie, Jerome Mutterer, Institute de Biologie Moleculaire des Plantes, Strasbourg, France). The threshold was set to the mean of the background plus three times the standard deviation. Pixels with the same coordinates in the two fluorescence images were regarded as colocalized when intensity values were above the respective threshold in both images. Images of the two detection channels were merged, and colocalized pixels were highlighted in white.

2.10. Translocation analysis

The translocation of LY across GUV membranes was analyzed by ImageJ [23]. Generally, GUVs with a radius R smaller than 20 μm were excluded from analysis. To identify the GUVs for the analysis, an intensity threshold was defined that separated the GUVs (low intensity) from the remaining solution (high intensity). This worked well since the intensity difference between GUV interior and exterior was usually high at the beginning of the measurement. The GUVs were then identified using the particle analysis tool of ImageJ. For these GUVs mean intensity values for their interior, F_{in}, were determined, and also the fluorescence intensity outside the GUVs, F_{out}. The ratio F_{in}/F_{out} was used as a measure for membrane permeation. This ratio was determined for all GUVs at certain time points after nisin incubation starts. Finally, the ratios were plotted in histograms presenting the data of at least 30 analyzed GUVs for each experimental condition. Significance of the data was tested with an independent, two-sample *t*-test. p-Values were calculated by the use of Matlab (MathWorks, Ismaning, Germany) and significance indicated in the diagram by labeling the respective bars with asterisks (three asterisks for $p < 0.005$, two asterisks for $p < 0.01$ and one asterisk for $p < 0.1$).

2.11. Aggregate analysis

Analysis of nisin–AF647 aggregates on GUV membranes was performed by the use of ImageJ and a dedicated Matlab routine (MathWorks, Ismaning, Germany). First, images were linearized along the equatorial membrane of the GUVs with the ImageJ polar transformer plugin (authored by Edwin Donnelly, Vanderbilt University School of Medicine, Nashville, USA and Frederic Mothe, Centre INRA de Nancy, Champenoux, France). Thereby, the circular intensity profile of the membrane was converted into a linear profile. The distribution of the intensity values along this line was determined, and fitted by a Gaussian function. The obtained values for the mean, $\overline{F}$, and the standard variation, σ, were used for normalization of the intensity values according to $F_n = (F - \overline{F}) / \sigma$. In the next step, molecular aggregates were identified as peaks in the normalized intensity profile by $F_n > 3$. The peak intensity value was related to the number of fluorescent molecules in the detected aggregate, and could therefore be used as a measure for the cluster size. From the number of peaks along the circular GUV profile the aggregate density per membrane length was calculated. Normalization, peak identification and cluster analysis were automatically performed by the Matlab routine. Generally, the equatorial membrane sections of more than 20 GUVs were evaluated for each experimental condition. Significance of the data was tested as described in Section 2.10.

3. Results

GUVs represent a well controllable membrane model system, and are well suited to systematically monitor the action of membrane active peptides on bilayers and therein incorporated receptors [22,24]. We examined the interaction of fluorescently labeled nisin with pure phospholipid GUVs and also GUVs that contained the target molecule of nisin, Lipid II, or one of its derivates by optical sectioning microscopy. In the beginning, we verified that the activity of labeled and unlabeled nisin did not differ significantly by means of a carboxyfluorescein leakage assay (Fig. S1). Indeed, the activity of the labeled molecule was slightly higher than that of the unlabeled species.

3.1. Interaction of nisin with pure phospholipid GUVs and GUVs containing Lipid II

Firstly, we investigated the non-specific interactions of nisin with membranes in order to discriminate them from specific effects due to binding to targets such as Lipid II. We incubated GUVs prepared from DOPC and DOPC/DOPG in glucose solutions containing 1.5 μM red-fluorescent nisin–AF647. Interaction of nisin–AF647 with the GUVs was observed by CLSM in the equatorial plane directly after mixing and within less than 5 min incubation. For GUVs made from neutral DOPC all nisin–AF647 remained in the solution, which was indicated by the bright fluorescence outside the GUVs. No binding of nisin–AF647 to the GUV surface was observed (Fig. 2A). In contrast to this, for GUVs comprising DOPC and 20% negatively charged DOPG instantaneous binding of nisin–AF647 to the membrane was seen as the

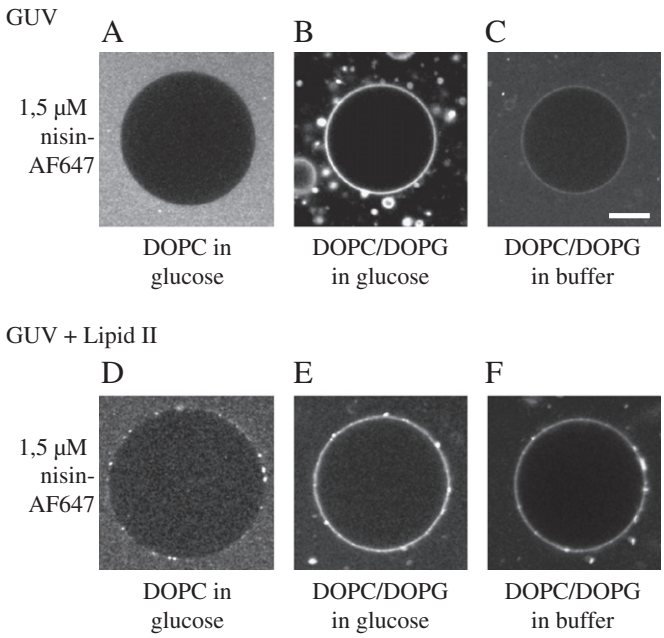

Fig. 2. Charge-driven and specific interaction of nisin–AF647 with phospholipid GUVs. Confocal images of nisin–AF647 at 1.5 μM acting on GUVs: (A) DOPC membranes in glucose solution, (B) DOPC/DOPG (80/20) membranes in glucose solution, and (C) DOPC/DOPG (80/20) membranes in buffer. In (D) to (F) GUVs contained 0.2 mol% Lipid II: (D) DOPC membranes in glucose solution, (E) DOPC/DOPG (80/20) membranes in glucose solution, and (F) DOPC/DOPG (80/20) membranes in buffer. GUVs were imaged at 5 min after incubation starts. Scale bar, 20 μm.

membrane showed a bright fluorescence signal and no fluorescence emanated from the surrounding solution (Fig. 2B). Furthermore, we observed numerous small liposomes in the solution (Fig. 2B), probably due to a decomposition of GUVs as a consequence of peptide accumulation on the membrane. When the experiment was repeated in buffer solution, accumulation of nisin on the GUV surface and also vesicle decomposition were largely reduced (Fig. 2C). Reduction of peptide binding was indicated by a considerably weaker fluorescence signal from the membrane and stronger fluorescence from the GUV environment compared to the incubation in sugar solution. Obviously, in the presence of ions, membrane and peptide charges were shielded, which reduced the effective attractive electrostatic forces between the negatively charged membrane and the positively charged peptide with its net charge of +3.

Next, we prepared GUVs containing Lipid II (0.2 mol%). In contrast to neutral, pure DOPC GUVs, Lipid II-containing DOPC GUVs in glucose solution rapidly bound nisin–AF647 (Fig. 2D). Accordingly, only fluorescence was observed from peptides in solution. Notably, in contrast to charge-induced interactions (Fig. 2B), membrane binding was not homogeneous, but bright fluorescent patches of nisin–AF647 appeared on the GUV membranes, which indicated the formation of large molecular aggregates. In order to examine whether the aggregates contained both nisin and Lipid II we used dual color fluorescence. When integrated in DOPC liposomes, green fluorescent Lipid II-Atto488 was homogeneously distributed in the GUV bilayer before addition of nisin, but following addition of nisin–AF647 it formed aggregates (Fig. 3). Colocalization analysis clearly indicated that the aggregates contained both nisin–AF647 and Lipid II-Atto488. We concluded that the specific binding of nisin to Lipid II results in the rapid formation of large-scale molecular nisin–Lipid II-aggregates in the GUV membrane. Interestingly, the image of the transmitted light channel showed that exactly at the location of the larger aggregates small vesicles formed (indicated by arrows in Fig. 3B) that were released from the GUVs.

When anionic GUVs (80% DOPC, 20% DOPG) were supplemented with Lipid II (0.2 mol%) and incubated in nisin–AF647–glucose solution, a mixture of unspecific and specific binding occurred: due to electrostatic forces nisin attached homogeneously to the negative charges of the membrane, but was also specifically binding to Lipid II. Again, this was indicated by the formation of membrane aggregates (Fig. 2E). The presence of ions slightly reduced the charge-driven binding to the membrane, but did not affect the formation of aggregates (Fig. 2F).

3.2. Nisin caused membrane permeability

Since it was not feasible to evaluate the permeation of the GUV membrane by the analysis of the nisin signal due to the strong membrane accumulation that usually occurred, we examined membrane permeation induced by nisin by using a small hydrophilic tracer dye, LY. LY exhibits a Stokes diameter of 1.2–1.5 nm, which is smaller than the previously reported diameter of pores formed by nisin and Lipid II [12]. For these translocation experiments, GUVs were incubated with nisin–AF647 at a concentration of 200 nM. This concentration was low enough to be in the nanomolar range of the nisin MIC, and still high enough for proper visualization of the interactions of nisin–AF647 with GUVs by confocal microscopy. Thus, we were able to correlate nisin binding and membrane permeation in terms of tracer translocation.

We followed the intensity distribution of the tracer fluorescence inside and outside of GUVs for various experimental conditions for 15 min upon application of nisin–AF647. As a permeability measure we used the ratio of the tracer fluorescence intensity inside, F_{in}, and outside the GUVs, F_{out}. For equilibration of the tracer, the ratio F_{in}/F_{out} equals 1. The ratio was determined for a set of vesicles as a function of incubation time. Fig. 4A shows the tracer fluorescence, when nisin acted on Lipid II-containing GUVs, for one representative experiment. We noticed that the response of the GUVs to nisin was very heterogeneous. In the lower panel of Fig. 4A we plotted the ratio of the tracer fluorescence

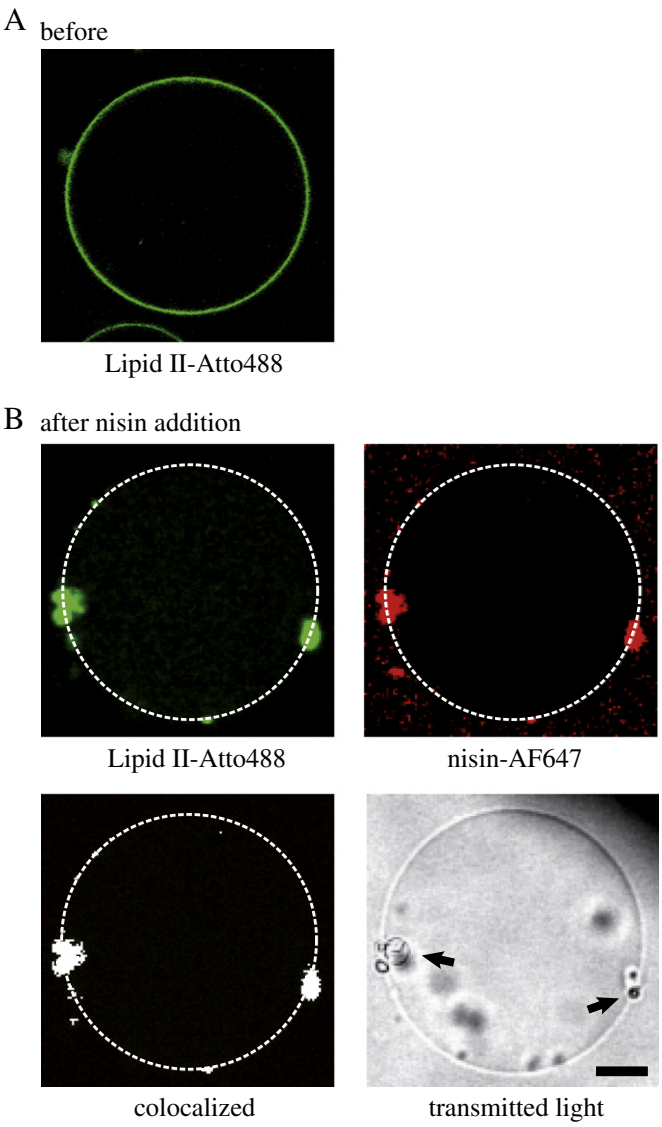

Fig. 3. Aggregation of Lipid II-Atto488 and nisin–AF647. Membrane distribution of Lipid II in DOPC GUVs containing 0.2 mol% Lipid II-Atto488 before addition of nisin (A) and after incubation in 250 mM glucose solution containing 200 nM nisin–AF647 (B). White pixels in the merged image mark colocalized nisin–AF647 and Lipid II-Atto488. The transmitted light image revealed the formation of small vesicles at the location of the nisin–Lipid II aggregates (see arrows). GUVs were imaged after 5 min incubation with nisin. Scale bar, 10 μm.

for GUVs of repeated experiments in histogram form. Obviously, the number of permeabilized GUVs (with $F_{in}/F_{out} \approx 1$) increased with time. In order to present the results of these permeation experiments in a more compact form we determined the mean values of the ratios in these histograms, and plotted them as a function of time (Fig. 4B).

In the presence of nisin an increase of permeability over time was observed for all membrane compositions (Fig. 4B). For pure phospholipid GUVs the effect of 200 nM nisin was relatively small. For both DOPC and DOPC/DOPG GUVs only a small increase in membrane permeability with time was observed. A comparable permeation level was seen at the start of the experiment, and a similar dependence on incubation time was observed. At the used concentration in the MIC range nisin did not affect membrane intactness neither in neutral nor in negatively charged GUVs significantly.

The situation was very different, when the GUV membrane contained Lipid II or further molecules that are known to be nisin

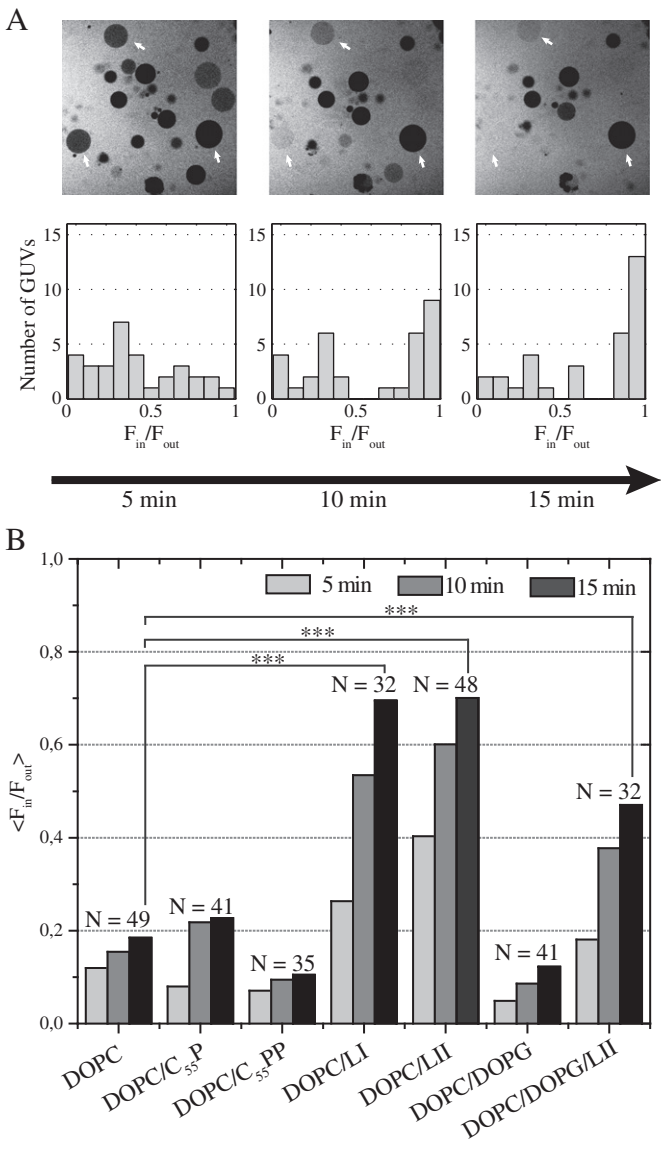

Fig. 4. Membrane permeation activity of nisin. In all experiments the fraction of bactoprenol components was 0.2 mol% and of DOPG 20 mol%. GUVs were incubated in 250 mM glucose solution containing 200 nM nisin–AF647 and 30 μM LY. (A) Time series of DOPC-GUVs containing Lipid II. The upper panel displays the intensity distribution of LY at the time points 5 min, 10 min and 15 min after nisin addition. White arrows indicate three vesicles which exhibit differing permeability kinetics. The lower panel shows the distribution of the intensity ratio F_{in}/F_{out} at the respective time points. For the histograms in (A) values of 48 liposomes were evaluated. (B) Mean ratios for different membrane compositions were calculated at the respective time points. Permeability increased over time. The independent, two-sample *t*-test, executed for ratios measured after 15 min, yielded p-values < 0.001 for Lipid I- and Lipid II-containing vesicles compared to DOPC vesicles (indicated by three asterisks at bars). Permeability was not significant for other mixtures.

targets. We examined all membrane bound members of the bactoprenol-Lipid II cycle in order to specify exactly, what the most effective target of nisin was. All results were summarized in Fig. 4B.

As expected from the previous results, nisin caused a strong membrane permeability of Lipid II-containing GUVs. Also, the permeability was reduced, when negatively charged Lipid II-containing GUVs made from DOPC and DOPG were studied. Then, the effect of nisin was clearly less pronounced than on neutral GUVs. Lipid I-containing GUVs were permeabilized by nisin almost as potently as Lipid II-containing GUVs. Again, this was expected, since the pyrophosphate binding site of Lipid I possesses the same chemical environment as in Lipid II, namely the isoprene chain on one side and N-acetylmuramic acid with the pentapeptide chain on the other side, which seems to attract nisin interaction in almost the same way for Lipid I and Lipid II. On the other hand, C_{55}-P containing GUVs did not show a greater permeabilization than that of neutral and anionic GUVs. This was not surprising, since the phosphate headgroup of C_{55}-P is not a binding site for nisin in contrast to C_{55}-PP-containing GUVs. For these, no increased membrane permeability was observed at all, although nisin was known to bind the pyrophosphate of C_{55}-PP [15]. Indeed, a failure to induce membrane permeation upon nisin binding to C_{55}-PP had also been observed before for small vesicles [25]. Obviously, binding of nisin alone was not sufficient to lead to membrane permeation. Therefore, we decided to examine, whether the characteristic aggregation that had been observed upon nisin binding to Lipid II, could be observed for C_{55}-PP as a consequence of the nisin interaction.

3.3. Nisin effect on different bactoprenol derivatives

Using fluorescent nisin enabled us to analyze the aggregates in terms of size, since this was related to the fluorescence intensity of the aggregates. Furthermore, by confocal imaging of respectively prepared GUVs the number of aggregates per unit length along the membrane equator could be determined, and was used as a measure for the general aggregate surface density.

By confocal imaging a 2-dimensional, equatorial section of the GUVs with an axial depth of about 1 μm can be mapped. For the quantitative analysis of nisin binding and aggregation this ring-shaped profile was linearized. Fig. 5A shows different exemplary GUV sections, which demonstrate the different types of nisin interaction that were observed. For neutral DOPC vesicles no binding was observed (Fig. 5A, upper image, see also Fig. 2A), whereas for DOPC/DOPG-GUVs strong and homogeneous binding occurred (Fig. 5A, central image, see also Fig. 2B). Lipid II-containing GUVs showed a third situation. There, the section revealed fluctuating intensities along the membrane due to strong nisin–AF647 aggregation (Fig. 5A, lower image, see also Fig. 2D). For the three examples, pixel intensity values were determined along the membrane and plotted in a histogram (Fig. 5B). The various intensity distributions of nisin–AF647 illustrate the differences in nisin–membrane interaction. A Gaussian-like distribution was obtained when nisin was not interacting with the GUVs (Fig. 5B, blue bars) and also, but at higher intensities, when nisin was homogeneously bound to the membrane through charge-driven interactions (Fig. 5B, green bars), but not in the case of aggregate formation (Fig. 5B, red bars). Here, a number of bars did not fit into the normal distribution, but occurred at higher intensities. These intensities corresponded to the nisin–AF647 aggregates. As described in the Material and methods the intensity distributions were fitted by a Gaussian function. With the thus determined mean and standard deviation the intensity profiles were normalized (Fig. 5C). The intensity profiles show that for the DOPC membrane (Fig. 5C, blue line) and for the DOPC/DOPG-GUV membrane (Fig. 5C, green line) all values lie around the baseline (Fig. 5C, black line) under a certain threshold (Fig. 5C, dashed line). Only the profile for the Lipid II-containing membrane showed pronounced peaks above the threshold. These peaks, referring to nisin aggregates, could well be detected and quantified by a Matlab software program (see Material and methods). To determine the size of the aggregates, we calculated the mean peak intensity for each sample from at least 15 GUVs. In addition, the analysis yielded the aggregate number per unit membrane length respectively the aggregate density (Fig. 5D).

We quantified the aggregates for all GUV types that were examined above, and found that Lipid II-containing GUVs exhibited the highest density of nisin aggregates, and also, with Lipid I-containing GUVs, the largest ones (Fig. 5D). For Lipid II-, Lipid I- and C_{55}-PP-containing GUVs a similar aggregate density was found, which was significantly higher than that of C_{55}-P-containing, DOPC/DOPG and DOPC GUVs. However, the aggregate sizes for Lipid II and Lipid I were significantly larger

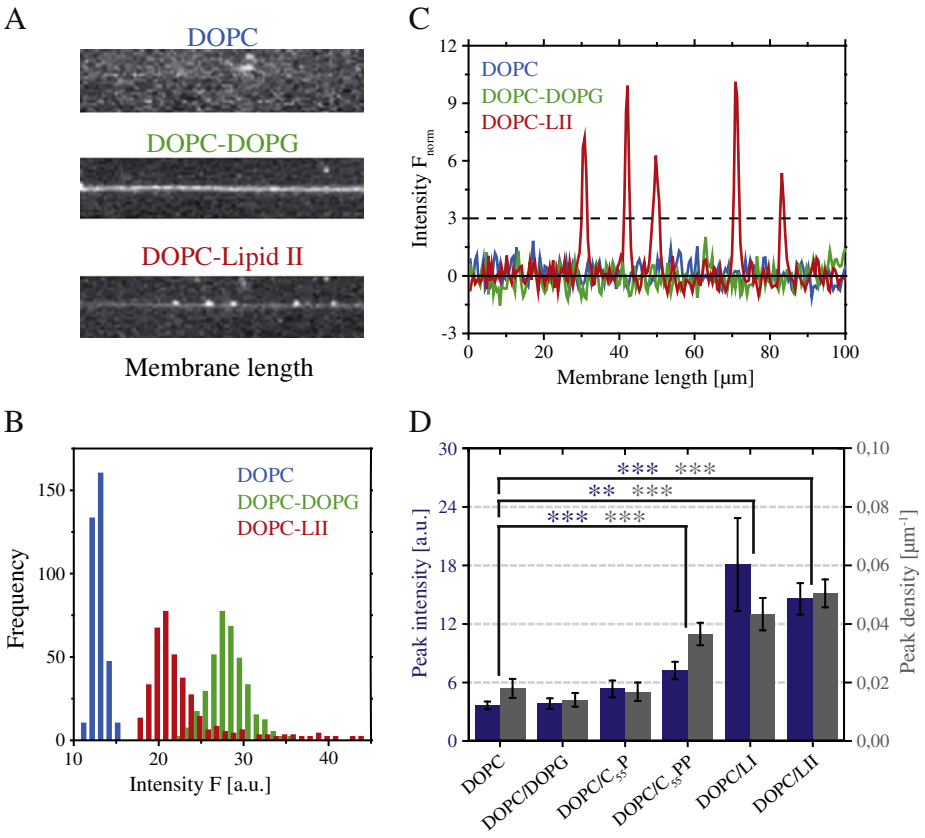

Fig. 5. Quantification of nisin–AF647 clustering in GUV membranes. (A) Linearized profile of the nisin–AF647 fluorescence signal along the membrane of GUVs of different composition as indicated (incubation time, 5 min); (B) histogram representation of the fluorescence intensity values along the line profiles shown in (A); (C) plot of the normalized intensity values along the GUV membranes shown in (A). Nisin–AF647 clusters showed significantly higher intensity values (red) than the baseline intensity (full black line, defined as zero). The dashed black line indicates the threshold intensity of 3*σ. (D) Mean peak intensities (blue) and mean aggregate densities (gray) for different GUV-phospholipid and bactoprenol compositions. Standard errors of the mean are given by error bars. At least 15 GUVs for each membrane composition were analyzed (DOPC: N = 24, DOPC/DOPG: N = 20, DOPC/C_{55}-P: N = 19, DOPC/C_{55}-PP: N = 28, DOPC/Lipid I: N = 15, DOPC/Lipid II: N = 21). Significance was tested (independent, two-sample *t*-test) between the values determined for negatively charged and bactoprenol-containing membranes and the values determined for DOPC membranes. When significant, it was indicated by asterisks (*** for $p < 0.005$ and ** for $p < 0.01$).

compared to C_{55}-PP (Lipid II: p-value < 0.005; Lipid I: p-value < 0.1). A size difference was also observed between C_{55}-P and C_{55}-PP aggregates. C_{55}-PP aggregates were significantly larger than those occurring in DOPC membranes, whereas C_{55}-P aggregates were not (Fig. 5D). As anticipated, for GUVs made from pure DOPC, DOPC/DOPG, and DOPC containing C_{55}-P the aggregates induced by nisin were small in size and number.

In summary, for all GUV mixtures that allowed only non-specific nisin interactions, small clusters and a low density were observed. In all mixtures that contained specific binding partners for nisin and for which nisin-induced membrane permeation was observed, large molecular aggregates were seen. Interestingly, the mean peak intensities of the aggregates induced by nisin in Lipid I- and Lipid II-containing GUVs were comparable. Obviously, approximately the same number of nisin molecules was accumulated in these clusters. This suggested that a specific process inhibited a further growth of the clusters. Examination of the images shown in Figs. 2D to F, 3 and 5A indicated that this process could be a pinch-off of small vesicles containing nisin aggregates.

4. Discussion

Lipid II with its central role in building the bacterial cell wall belongs to the important targets of many classes of current antibiotics [26]. Here, we focused on the effect of the lantibiotic nisin on Lipid II and its bactoprenol precursors. To this end, we incorporated the various bactoprenol derivatives in GUV membranes and studied membrane perforation and bactoprenol aggregation induced by nisin in a quantitative manner. The goal of this study was to improve our understanding of the mode of action of the lantibiotic nisin.

Previously, it was shown in model membrane studies that nisin destroys the membrane of small unilamellar vesicles (SUVs) at micromolecular concentrations [7]. When applied at such concentrations the peptide was by one order of magnitude more effective in perforating negatively charged compared to neutral membranes demonstrating that membrane charge is important for the direct interaction of nisin with membranes. This was corroborated by AFM studies on planar model membranes, on which nisin at 1.5 μM generated micellar or vesicular associates upon contact with anionic, but not with neutral membranes [27]. In most of our experiments, however, nisin was applied at a concentration of 200 nM only. This concentration was chosen such that nisin would bind the majority of Lipid II molecules, when present in the membrane, because the respective dissociation constant is 50 nM [27]. Also, this value was in the range of the MIC of nisin against Gram-positive bacteria [8].

As expected we found that a negative membrane charge enhanced peptide accumulation at the GUV membrane, but a significant membrane perforation did not occur for neutral or negatively charged GUVs at 200 nM. This result confirmed that charge-driven membrane permeabilization of nisin is concentration dependent, and does not play a major role in the range of the biologically relevant MIC.

The specific interaction of nisin with Lipid II-comprising GUVs yielded distinctly different effects. Nisin binding to Lipid II provoked a drastic change of the Lipid II distribution in the membrane. Lipid II accumulated in large complexes together with nisin as was assumed in a previous study *in vitro* and *in vivo* [14]. Here, we explicitly demonstrated for the first time that the aggregates induced by nisin contain both large numbers of nisin and Lipid II molecules by colocalizing respectively fluorescently labeled molecules. It can be anticipated that this is also the case for the other examined bactoprenol derivatives. For Lipid II, aggregation was accompanied by membrane permeation, which was shown by the influx of tracer molecules with a diameter of 1.5 nm into the GUVs.

The amount of permeation differed greatly between single GUVs. Large differences between individual GUVs were generally observed in our kinetic measurements. We assume that this was due to the fact that the formation of membrane perforations by amphipathic peptides is a stochastic process and highly dependent on local peptide concentrations [28]. A negative charge in Lipid II-containing GUVs decreased the permeation activity of nisin probably because two components, the anionic lipid head group and Lipid II, competed for nisin [27].

Nisin bound to and formed aggregates also with Lipid I, and perforated the membrane similar as upon interaction with Lipid II. This was expected since Reisinger and coworkers discovered already in 1980 that nisin forms complexes with Lipid I thus inhibiting Lipid II synthesis [29]. However, Lipid I is not a primary target of nisin *in vivo* since it resides on the cytoplasmic face of bacterial membranes. But due to the demonstrated membrane permeation translocation of nisin across the cell membrane is possible and Lipid I may probably also be targeted.

Hsu and coworkers unambiguously demonstrated the central role of Lipid II's pyrophosphate group for the interaction with nisin [15], but also stated that it is presumably a necessary, but not a sufficient determinant. In agreement with this no specific interaction with C_{55}-P, but with C_{55}-PP was detected, even though the affinity of nisin for Lipid II was found to be twice as high [30]. Interestingly, in our direct visualization of GUV membranes we observed that nisin formed aggregates when C_{55}-PP was present in the membrane, but the aggregates were clearly smaller than those formed with Lipids I and II. Remarkably, the nisin–C_{55}-PP aggregates left the membrane intact, whereas the membrane was perforated by nisin–Lipid I and nisin–Lipid II aggregates very effectively. For Lipids I and II, whose interaction with nisin resulted in membrane perforation, the same mean cluster size was observed. We suspect that a quorum of assembled molecules was required for an efficient membrane perforation.

Several recent molecular dynamics simulations of the action of bioactive peptides revealed the importance of the distortion of membrane topology by membrane-active peptides for creating membrane pores or large-scale membrane perforations [31,32]. In these simulations it was found that the bioactive maculatin 1.1 or TAT peptides induced a negative membrane curvature, and magainin 2 even provoked vesicle budding [33]. We suspect that this is also the case for Lipid II-bound nisin, as we generally observed the formation of small vesicles at the locations of Lipid II–nisin aggregates. This observation suggests a major role for large-scale alterations of the membrane topology during the perforation process. Of course, it remains to be shown that such vesicle budding upon nisin addition also occurs *in vivo*, possibly at least partially.

In the seemingly simple nisin–Lipid II system we encountered a remarkable biophysical effect. Binding of an effector molecule – nisin – to its membrane-anchored target caused the dramatic and large-scale aggregation of the latter — C_{55}-PP, Lipid I or Lipid II. The physical driving force for this aggregation process is still quite unclear. It is not probable that it is due to direct molecular interactions, because these would lead only to the formation of multimers of limited size — but not to the formation of light-microscopically visible molecular aggregates comprising hundreds or thousands of molecules. Molecular dynamics simulations similar to those that were recently performed to study the Lipid II–vancomycin interaction and its consequences for the lipid bilayer properties would probably contribute to a physical understanding of the membrane-associated aggregation process [34]. The driving force acting in this simple molecular system is of greatest importance for understanding the action principle of lantibiotics. Possibly, it is also of importance for further signaling processes involving membrane receptors responding to their signals.

Supplementary data to this article can be found online at http://dx.doi.org/10.1016/j.bbamem.2013.07.014.

Acknowledgements

We gratefully acknowledge funding by the German Research Foundation through the Collaborative Research Centre SFB 624 “Templates — Functional Chemical Matrices” and through the FOR 854, project TP4. K.S. was supported by the Cusanuswerk. C.C. was supported by the European Commission's 6th Framework Program through the Marie-Curie Action BIOCONTROL, contract number MCRTN — 33439.

References

[1] A.T.R. Mattick, A. Hirsch, Further observations on an inhibitory substance (nisin) from lactic streptococci, Lancet 253 (1947) 5–8.
[2] M.K. Rayman, B. Aris, A. Hurst, Nisin: a possible alternative or adjunct to nitrite in the preservation of meats, Appl. Environ. Microbiol. 41 (1981) 375–380.
[3] E. Gross, J.L. Morell, The structure of nisin, J. Am. Chem. Soc. 93 (1971) 4634–4635.
[4] H. Brötz, M. Josten, I. Wiedemann, U. Schneider, F. Götz, G. Bierbaum, H.G. Sahl, Role of lipid-bound peptidoglycan precursors in the formation of pores by nisin, epidermin and other lantibiotics, Mol. Microbiol. 30 (1998) 317–327.
[5] P.M. Hwang, H.J. Vogel, Structure–function relationships of antimicrobial peptides, Biochem. Cell Biol. 76 (1998) 235–246.
[6] E. Ruhr, H.G. Sahl, Mode of action of the peptide antibiotic nisin and influence on the membrane potential of whole cells and on cytoplasmic and artificial membrane vesicles, Antimicrob. Agents Chemother. 27 (1985) 841–845.
[7] I. Wiedemann, E. Breukink, C. van Kraaij, O.P. Kuipers, G. Bierbaum, B. de Kruijff, H.G. Sahl, Specific binding of nisin to the peptidoglycan precursor lipid II combines pore formation and inhibition of cell wall biosynthesis for potent antibiotic activity, J. Biol. Chem. 276 (2001) 1772–1779.
[8] W. Brumfitt, M.R. Salton, J.M. Hamilton-Miller, Nisin, alone and combined with peptidoglycan-modulating antibiotics: activity against methicillin-resistant *Staphylococcus aureus* and vancomycin-resistant enterococci, J. Antimicrob. Chemother. 50 (2002) 731–734.
[9] T. Schneider, H.G. Sahl, An oldie but a goodie — cell wall biosynthesis as antibiotic target pathway, Int. J. Med. Microbiol. 300 (2010) 161–169.
[10] T. Mohammadi, V. van Dam, R. Sijbrandi, T. Vernet, A. Zapun, A. Bouhss, M. Diepeveen-de Bruin, M. Nguyen-Disteche, B. de Kruijff, E. Breukink, Identification of FtsW as a transporter of lipid-linked cell wall precursors across the membrane, EMBO J. 30 (2011) 1425–1432.
[11] A. Lamsa, W.T. Liu, P.C. Dorrestein, K. Pogliano, The *Bacillus subtilis* cannibalism toxin SDP collapses the proton motive force and induces autolysis, Mol. Microbiol. 84 (2012) 486–500.
[12] I. Wiedemann, R. Benz, H.G. Sahl, Lipid II-mediated pore formation by the peptide antibiotic nisin: a black lipid membrane study, J. Bacteriol. 186 (2004) 3259–3261.
[13] H.E. Hasper, B. de Kruijff, E. Breukink, Assembly and stability of nisin–lipid II pores, Biochemistry 43 (2004) 11567–11575.
[14] H.E. Hasper, N.E. Kramer, J.L. Smith, J.D. Hillman, C. Zachariah, O.P. Kuipers, B. de Kruijff, E. Breukink, An alternative bactericidal mechanism of action for lantibiotic peptides that target lipid II, Science 313 (2006) 1636–1637.
[15] S.T. Hsu, E. Breukink, E. Tischenko, M.A. Lutters, B. de Kruijff, R. Kaptein, A.M. Bonvin, N.A. van Nuland, The nisin–lipid II complex reveals a pyrophosphate cage that provides a blueprint for novel antibiotics, Nat. Struct. Mol. Biol. 11 (2004) 963–967.
[16] O.P. Kuipers, H.S. Rollema, W.M.G.J. Yap, H.J. Boot, R.J. Siezen, W.M. Devos, Engineering dehydrated amino-acid-residues in the antimicrobial peptide nisin, J. Biol. Chem. 267 (1992) 24340–24346.
[17] I. Wiedemann, R.R. Bonelli, T. Schneider, H.G. Sahl, Insights into in vivo activities of lantibiotics from gallidermin and epidermin mode-of-action studies, Antimicrob. Agents Chemother. 50 (2006) 1449–1457.
[18] T. Schneider, M.M. Senn, B. Berger-Bachi, A. Tossi, H.G. Sahl, I. Wiedemann, In vitro assembly of a complete, pentaglycine interpeptide bridge containing cell wall precursor (lipid II-Gly5) of *Staphylococcus aureus*, Mol. Microbiol. 53 (2004) 675–685.
[19] U. Kohlrausch, J.V. Holtje, One-step purification procedure for UDP-N-acetylmuramyl-peptide murein precursors from *Bacillus cereus*, FEMS Microbiol. Lett. 78 (1991) 253–258.
[20] D.S. Dimitrov, M.I. Angelova, Lipid swelling and liposome formation mediated by electric fields, Bioelectrochem. Bioenerg. 19 (1988) 323–336.
[21] F.M. Menger, J.S. Keiper, Giant vesicles: micromanipulation of membrane bilayers, Adv. Mater. 10 (1998) 888–890.
[22] C. Ciobanasu, E. Harms, G. Tünnemann, M.C. Cardoso, U. Kubitscheck, Cell-penetrating HIV1 TAT peptides float on model lipid bilayers, Biochemistry 48 (2009) 4728–4737.
[23] C.A. Schneider, W.S. Rasband, K.W. Eliceiri, NIH Image to ImageJ: 25 years of image analysis, Nat. Methods 9 (2012) 671–675.

[24] C. Ciobanasu, J.P. Siebrasse, U. Kubitscheck, Cell-penetrating HIV1 TAT peptides can generate pores in model membranes, Biophys. J. 99 (2010) 153–162.
[25] B.B. Bonev, E. Breukink, E. Swiezewska, B. De Kruijff, A. Watts, Targeting extracellular pyrophosphates underpins the high selectivity of nisin, FASEB J. 18 (2004) 1862–1869.
[26] T. Schneider, H.G. Sahl, Lipid II and other bactoprenol-bound cell wall precursors as drug targets, Curr. Opin. Investig. Drugs 11 (2010) 157–164.
[27] K. Christ, I. Wiedemann, U. Bakowsky, H.G. Sahl, G. Bendas, The role of lipid II in membrane binding of and pore formation by nisin analyzed by two combined biosensor techniques, Biochim. Biophys. Acta 1768 (2007) 694–704.
[28] M.T. Lee, W.C. Hung, F.Y. Chen, H.W. Huang, Mechanism and kinetics of pore formation in membranes by water-soluble amphipathic peptides, Proc. Natl. Acad. Sci. U. S. A. 105 (2008) 5087–5092.
[29] P. Reisinger, H. Seidel, H. Tschesche, W.P. Hammes, The effect of nisin on murein synthesis, Arch. Microbiol. 127 (1980) 187–193.
[30] A. Müller, H. Ulm, K. Reder-Christ, H.G. Sahl, T. Schneider, Interaction of type A lantibiotics with undecaprenol-bound cell envelope precursors, Microb. Drug Resist. 18 (2012) 261–270.
[31] P.J. Bond, D.L. Parton, J.F. Clark, M.S. Sansom, Coarse-grained simulations of the membrane-active antimicrobial peptide maculatin 1.1, Biophys. J. 95 (2008) 3802–3815.
[32] A. Mishra, V.D. Gordon, L. Yang, R. Coridan, G.C. Wong, HIV TAT forms pores in membranes by inducing saddle-splay curvature: potential role of bidentate hydrogen bonding, Angew. Chem. Int. Ed Engl. 47 (2008) 2986–2989.
[33] H.J. Woo, A. Wallqvist, Spontaneous buckling of lipid bilayer and vesicle budding induced by antimicrobial peptide magainin 2: a coarse-grained simulation study, J. Phys. Chem. B 115 (2011) 8122–8129.
[34] Z. Jia, M.L. O'Mara, J. Zuegg, M.A. Cooper, A.E. Mark, The effect of environment on the recognition and binding of vancomycin to native and resistant forms of lipid II, Biophys. J. 101 (2011) 2684–2692.